Title

Extracellular Polymeric Substance Architecture Influences Natural Genetic Transformation of Acinetobacter baylyi in Biofilms

Journal

Applied and Environmental Microbiology, 80(24)

ISSN

0099-2240

Authors

Merod, Robin T

Wuertz, Stefan

Publication Date

2014-12-15

DOI

10.1128/aem.01984-14

Peer reviewed

AEM
Journals.ASM.org

Extracellular Polymeric Substance Architecture Influences Natural Genetic Transformation of *Acinetobacter baylyi* in Biofilms

Robin T. Merod,[a] Stefan Wuertz[a,b,c]

Department of Civil and Environmental Engineering, University of California, Davis, California, USA[a]; Singapore Centre on Environmental Life Sciences Engineering, Nanyang Technological University, Singapore[b]; School of Civil and Environmental Engineering, Nanyang Technological University, Singapore[c]

Genetic exchange by natural transformation is an important mechanism of horizontal gene transfer in biofilms. Thirty-two biofilm metrics were quantified in a heavily encapsulated *Acinetobacter baylyi* strain and a miniencapsulated mutant strain, accounting for cellular architecture, extracellular polymeric substances (EPS) architecture, and their combined biofilm architecture. In general, transformation location, abundance, and frequency were more closely correlated to EPS architecture than to cellular or combined architecture. Transformation frequency and transformant location had the greatest correlation with the EPS metric surface area-to-biovolume ratio. Transformation frequency peaked when EPS surface area-to-biovolume ratio was greater than 3 $\mu m^2/\mu m^3$ and less than 5 $\mu m^2/\mu m^3$. Transformant location shifted toward the biofilm-bulk fluid interface as the EPS surface area-to-biovolume ratio increased. Transformant biovolume was most closely correlated with EPS biovolume and peaked when transformation occurred in close proximity to the substratum. This study demonstrates that biofilm architecture influences *A. baylyi* transformation frequency and transformant location and abundance. The major role of EPS may be to facilitate the binding and stabilization of plasmid DNA for cellular uptake.

Biofilms provide an optimal environment for the occurrence of horizontal gene transfer, for example, via natural genetic transformation, i.e., the active cellular uptake of free DNA. Free DNA, naturally originating from cell lysis or active cellular secretion (1), is a central component of biofilms (2) and has even been found in higher quantities than intercellular genomic DNA (3). The capacity of biofilms to incorporate DNA into their architecture prevents free DNA from escaping into the surrounding environment and potentially protects free DNA from degradation. Subsequently, the high microbial density of biofilms increases the probability that transformation-competent cells will come into contact with free DNA. The microorganism *Acinetobacter baylyi* strain ADP1 is a good experimental model for studying natural genetic transformation due to its naturally high competence (4). In contrast to planktonic cultures, its ability to form stable biofilms makes it the organism of choice to investigate genetic transformation as it may occur in the natural environment.

While nutrient conditions, biofilm maturity, and mode of growth (5–7) have been shown to affect natural genetic transformation in *A. baylyi* biofilms, the influence of biofilm architecture (that is, the biofilm's physical structure) has not been fully established. Biofilm architecture is integral to microbial life and influences the functional characteristics of the biofilm. For example, biofilm thickness, porosity, surface roughness, and cell cluster density contribute to mass transport limitations (8, 9), while interconnecting channels facilitate mass transport throughout the biofilm's depth (10, 11). In turn, mass transport affects localized microbial diversity in multispecies biofilms (12, 13), which subsequently determines the extent of metabolic capabilities. We hypothesized that biofilm architecture would also influence transformation frequency and transformant location and abundance.

Many studies investigating biofilm architecture structure-function relationships have focused on the microbial distribution but ignored extracellular polymeric substances (EPS), which exhibit a critical function in biofilms (14, 15). In this study, different architectures were induced in monoculture *A. baylyi* biofilms by controlling the number of biofilm-establishing cells and biofilm-developmental nutrient conditions. Additionally, the influence of EPS architecture was determined by using the heavily encapsulated strain BD4 and the miniencapsulated mutant strain ADP1 (16). Various metrics of cellular, EPS, and overall biofilm architecture were quantified *in situ* to elucidate their effect on natural genetic transformation.

MATERIALS AND METHODS

Bacterial strains, plasmids, and media. *Acinetobacter baylyi* strain BD4 and *A. baylyi* strain ADP1 (17), previously referenced as *Acinetobacter* sp. strain ADP1, were used as model biofilm-forming organisms. The plasmid pGAR38, a Mob^+ Tra^- gentamicin- and tetracycline-resistant IncQ plasmid, was used as the model DNA element for transformation. pGAR38 is pML10 (18) containing the wild-type green fluorescent protein (GFP) gene, *gfp* (Clontech, Palo Alto, CA), under the regulation of a P*psbA* promoter (19). Induction of the promoter was not necessary. Brain heart infusion (BHI) medium, mineral medium M9 (20), and 0.01 M $MgSO_4$ were used during transformation experiments.

Biofilm growth and transformation. Biofilms were grown in stainless steel, multilane flow cells previously described by Hendrickx et al. (21) under continuous flow conditions. The entire system was autoclaved prior to experimentation. Prior to flow cell inoculation, all cultures were washed three times in 1× phosphate-buffered saline (PBS) after having been grown overnight in BHI at 30°C. A 250-μl volume of washed cells containing either 10^7 or 10^9 cells was inoculated into flow cell lanes and allowed to settle for 2 h before starting continuous flow of the growth media listed in Table 1. All biofilms were grown with a flow rate of 2.5 ml/h in a constant-temperature chamber at 30°C.

Received 9 July 2014 Accepted 22 September 2014
Published ahead of print 10 October 2014
Editor: A. M. Spormann
Address correspondence to Stefan Wuertz, swuertz@ucdavis.edu.
This paper is dedicated to the memory of Larissa Hendrickx.

doi:10.1128/AEM.01984-14

TABLE 1 Biofilm developmental growth conditions and subsequent transformation frequency results

Growth medium	No. of cells[a]	Transformation frequency (10^{-3}) (mean ± SD[b])	
		BD4	ADP1
0.01% gluconate in M9	10^9	2.4 ± 1.6	0.42 ± 0.06
0.3% gluconate in M9	10^7	0.98 ± 0.15	0.96 ± 1.16
Brain heart infusion	10^9	2.8 ± 3.1	2.9 ± 2.6
Brain heart infusion	10^7	5.5 ± 5.1	19 ± 9

[a] Number of cells inoculated into flow chamber to initiate biofilm growth.
[b] The standard deviation was calculated from 21 scanned locations.

Each strain was subjected to four different growth conditions (Table 1) in order to manipulate the formation of architectural characteristics. For each growth condition, two biofilms were grown in the same flow cell to obtain replicate biofilm architectures prior to transformation (22). Biofilms were allowed to grow for 3 days prior to being washed of growth medium for 12 h with M9 containing no carbon source. Following the wash step, one of the two biofilms underwent transformation with 2.5 μg/ml of pGAR38 in M9 containing 0.2% pyruvate. The remaining biofilm was sacrificed to visualize the initial EPS and cellular architecture. For transformation, a 500-μl volume of plasmid-containing medium was pumped into flow channels equating to 1.25 μg pGAR38 applied over the time course of 12 min. The plasmid-containing medium was then switched to M9 containing 0.2% pyruvate without DNA to allow GFP expression and maturation. After 3 days, the biofilm was visualized for cells and transformants using confocal laser scanning microscopy (CLSM).

Biofilm staining and CLSM observation and image acquisition. Biofilms were stained under a continuous flow for 1 h and then washed with 0.01 M $MgSO_4$ for 30 min. Cells were stained with 5 μM Syto60 (Molecular Probes, Eugene, OR) suspended in 0.01 M $MgSO_4$. EPS was stained with 0.05% (by weight) Solophenyl flavine (SPF; Huntsman Int. LLC, High Point, NC) suspended in 0.01 M $MgSO_4$ and filtered using a 0.2-μm sterilization filter (23).

Flow cells were mounted on a Zeiss 510 META CLSM (Carl Zeiss, Jena, Germany) motorized stage and visualized using a 63×/1.2 numerical aperture (NA) (C-Apochromat) water immersion objective lens. Syto60-stained cells were scanned using a 633-nm helium laser with a 650-nm long-pass filter. EPS stained with SPF and GFP-expressing transformants were scanned using a 488-nm argon laser with a 505-nm long-pass filter.

Twenty-one CLSM image stacks were acquired from each biofilm to obtain a representative sample of architectural variation (24). Automatic acquisition was accomplished using the MultiTime Series (MTS) macro supplemental to Zeiss's CLSM interface software. Scanning locations were limited to the central 20-mm region of the flow lane to exclude entrance and exiting flow effects on biofilm architecture occurring 10 mm from the inlet and outlet. Scanning was also limited to 1.5 mm from the channel walls to exclude excessive biofilm accumulation. *z* stacks scanned from a single biofilm contained the same number of images. The number of images was set to capture the thickest part of the biofilm. Images had a pixel resolution of 0.2856 μm/pixel. The *z* step for images in a *z* stack was 0.75 μm. In accordance with optimal settings described by Sekar et al. (25), images were acquired utilizing a 1× digital magnification, a pinhole setting of 1 Airy unit, and a scan average of 2; the detector gain (500 to 550 arbitrary units), amplifier offset (0 to 0.05 arbitrary unit), and laser intensity (10% to 25%) were set to obtain adequately contrasted gray-scale images based on the brightest region of the biofilm that was scanned.

Image analysis. Semiautomated image analysis was performed utilizing the programs Auto PHLIP-ML (26) and PHLIP (27). Auto PHLIP-ML (available at http://sourceforge.net/projects/auto-phlip-ml/) calculates an Otsu threshold for image stacks not biased by extraneous images (images without pixels of biological significance). Extraneous images are identified and removed based on their area coverage of biomass as described by Merod et al. (26). The percent area coverage value used for extraneous image removal (PACVEIR) identifying the substratum was set at 1%. The bulk medium interface was defined by the limit of EPS and iteratively determined to have a PACVEIR of either 0% or 0.005%. PHLIP version 0.7, a MatLab-based image analysis toolbox (available at http://sourceforge.net/projects/phlip/), was used to quantify architectural metrics for each *z* stack. The Auto PHLIP-ML-calculated Otsu thresholds for transformant images were too low to obtain meaningful data, so the thresholds were set manually.

The following biofilm architectural metrics are included in PHLIP v0.7 and described by Mueller et al. (27). Biovolume is the volume of cellular biomass, transformant biomass, EPS biomass, or cellular-and-EPS (overall) biomass. The surface area-to-biovolume ratio is the surface area of the biomass divided by the biovolume. Mean thickness is the average thickness of the biomass. Roughness is a measure of how much the biomass thickness varies. Horizontal, vertical, and total spatial spreading is a characterization of the spreading of the biomass in space.

Scripts for the following architectural metrics were added to the single-channel and all-channel image processing operations of PHLIP. Porosity ($\mu m^3/\mu m^3$) is calculated as the difference between total volume and biovolume divided by the total volume, where total volume was calculated as the biomass mean thickness multiplied by the *z*-stack–*x*–*y* area. Maximum thickness (μm) is calculated as the number of images in the *z* stack multiplied by the *z* step (the μm distance between each image). Surface area (μm^2) is calculated as the product of biovolume and surface area-to-biovolume ratio. Normalized mean location (NML) of biomass is calculated as described by Hendrickx and Wuertz (5). Normalized mean location ranges from 0 (substratum) to 1 (biofilm-bulk medium interface) and provides a normalized *z* location for the majority of biomass.

$$\mathrm{NML} = \frac{\sum_{i=0}^{k} z_i \times (z_{i+1} - z_i) \times A_i}{V \times z_k}$$

where z_i is distance from the substratum at image i (μm), z_k is maximum thickness of biomass (μm), A_i is area coverage of biomass at image i (μm^2), and V is biovolume of biomass in the *z* stack (μm^3).

Architectural metrics were calculated for both the cellular component and EPS component of the biofilm using PHLIP's single-channel processing. The overall architecture for each metric was calculated using PHLIP's all-channel image processing, which superimposed the cellular channel and EPS channel. The three-dimensional (3D) colocalization of cells and transformants was defined to equal the transformation frequency (i.e., biovolume of transformants per biovolume of cells). The biovolume of transformants was calculated by multiplying the transformation frequency by the biovolume of cells.

Statistical analysis. The architecture of sacrificed biofilms was used to replicate the initial architecture (i.e., the architecture prior to transformation) of the biofilm used for transformation that developed under identical growth conditions. Three-way analysis of variance (ANOVA) was used on the initial architecture characteristics to determine if biofilms displayed significantly different architectures when grown under different medium conditions. The factors for the three-way ANOVA were biofilm type (eight levels: two *A. baylyi* strains each with four treatments [Table 1]), architectural component (three levels: cellular, EPS, and overall), and architecture metric (ten levels: biovolume, NML, porosity, mean thickness, roughness, horizontal spreading, vertical spreading, total spreading, surface area, and surface area-to-biovolume ratio). Each architectural metric had a sample number of 21. Based on this design, each biofilm type has three architectural components, and each architectural component has 10 architecture metrics. Therefore, the architecture of each biofilm type was quantified by 30 levels of measurement.

Spearman rank order analysis was used to determine which initial architecture metrics correlated with transformation frequency, transformant biovolume, or transformant NML. Each architectural metric had a sample number of 168, corresponding to 8 biofilms each with 21 *z* stacks.

TABLE 2 Transformation frequency Spearman rank order correlation results for significant architectural metrics[a]

Correlation level[b]	Metrics with indicated correlation (r_s; P)	
	Positive	Negative
Strong	None	None
Intermediate	None	None
Weak	3D coloc cellular EPS (0.38; <0.001); EPS biovolume (0.28; <0.001)	EPS SA:BV (−0.42; <0.001); EPS porosity (−0.27; <0.001); overall NML (−0.25; 0.001)

[a] Correlations with a P value less than 0.05 were considered to be significant. 3D coloc cellular EPS, three dimensional colocalization of cellular and EPS architecture; EPS, extracellular polymeric substances; NML, normalized mean location; SA:BV, surface area-to-biovolume ratio.

[b] r_s values were defined as having the following levels of correlation: $0.75 \leq r_s < 1$ and $-0.75 \geq r_s > -1$ were strong; $0.50 \leq r_s < 0.75$ and $-0.50 \geq r_s > -0.75$ were intermediate; $0.25 \leq r_s < 0.50$ and $-0.25 \geq r_s > -0.50$ were weak; and $-0.25 < r_s < 0.25$ had no correlation.

The Spearman rank order correlation coefficient (r_s) has a value range from +1 to −1. Coefficient values were defined to have the following level of correlation: $0.75 \leq r_s < 1$ and $-0.75 \geq r_s > -1$ were strong; $0.50 \leq r_s < 0.75$ and $-0.50 \geq r_s > -0.75$ were intermediate; $0.25 \leq r_s < 0.50$ and $-0.25 \geq r_s > -0.50$ were weak; and $-0.25 < r_s < 0.25$ had no correlation. Only correlations with a P value less than 0.05 were considered significant. Positive values had a positive correlation, and negative values had a negative correlation. SigmaStat version 3.5 (Systat Software, Inc.) was used for all statistical analyses.

RESULTS

Effect of growth conditions on biofilm architecture. To determine the role that biofilm architecture plays in natural genetic transformation, different architectures were induced. The wild-type strain *A. baylyi* strain BD4 and the miniencapsulated EPS mutant *A. baylyi* strain ADP1 were used to investigate the effect of differences in EPS. Additionally, different growth conditions were utilized during biofilm development to promote architectural differences between biofilms (Table 1). Brain heart infusion medium was chosen to provide a rich, unlimiting growth environment and promote a "fluffy" architecture, while M9 medium with different concentrations of gluconate was used to induce more dense biofilm architectures.

The architecture of each biofilm was quantified by 30 levels of measurement. Three-way ANOVA allowed us to evaluate if the eight biofilms had significant differences in architecture. The Tukey test on three-way-ANOVA results showed a significant difference in all biofilm pairwise comparisons ($P < 0.05$) except for two: ADP1_gluconate_10^9 versus BD4_BHI_10^9 and ADP1_BHI_10^7 versus BD4_gluconate_10^9 (biofilm names have the format "strain _growth medium_inoculation cell number"). On the basis of these results, we concluded that sufficient architectural variation exists to evaluate the effect of architecture on transformation frequency and location.

Effect of biofilm architecture on transformation frequency. The average transformation frequency ranged from 0.019 to 0.00042, measured as transformant biovolume per cellular biovolume (Table 1). As expected, the miniencapsulated mutant strain ADP1, which is known to be highly competent, exhibited the greatest transformation frequency. Cellular, EPS, and overall biofilm architecture were investigated to determine their influence on transformation frequency. Biofilm architecture was measured using 10 architectural metrics (see " Image analysis" in Materials and Methods). Additionally, 3D colocalization of cells and EPS and maximum thickness were examined, totaling a comparison of 32 architectural metrics. Five of the 32 metrics correlated weakly with transformation frequency (Table 2). No comparisons resulted in a strong or intermediate correlation. The EPS surface area-to-biovolume ratio was the most closely correlated, with an r_s value of −0.42 and a P value less than 0.001. Transformation frequency peaked when EPS surface area-to-biovolume ratio was greater than 3 $\mu m^2/\mu m^3$ but less than 5 $\mu m^2/\mu m^3$ (Fig. 1).

Effect of biofilm architecture on transformant biovolume. Transformant biovolume underwent the same Spearman rank order correlation analysis that was performed on transformation frequency. As with transformation frequency, transformant biovolume did not strongly correlate with any of the 32 architectural metrics. However, transformant biovolume had an intermediate correlation with EPS biovolume and EPS porosity. Nine other architectural metrics had a weak correlation (Table 3). In general, the metrics biovolume, porosity, and surface area for each aspect of biofilm architecture (i.e., cellular, EPS, and overall) were correlated with transformant biovolume. Transformant biovolume peaked when transformation occurred in close proximity to the substratum.

Effect of biofilm architecture on transformant location. As with transformation frequency and transformant biovolume, the same biofilm architecture metrics were investigated to determine their influence on transformant normalized mean location (NML). Twenty-one out of 32 metrics correlated with transformant NML (Table 4). The top five correlated metrics were all a measure of EPS architecture. The metric EPS surface area-to-biovolume ratio was strongly positively correlated (Fig. 2), while EPS NML (Fig. 3), porosity, total spreading, and vertical spreading were intermediately positively correlated. Of the remaining 16 comparisons, 14 (five cellular, two EPS, six overall architectural metrics, and maximum thickness) were weakly positively correlated to transformant NML and two were weakly negatively correlated (EPS biovolume and 3D colocalization of cells and EPS).

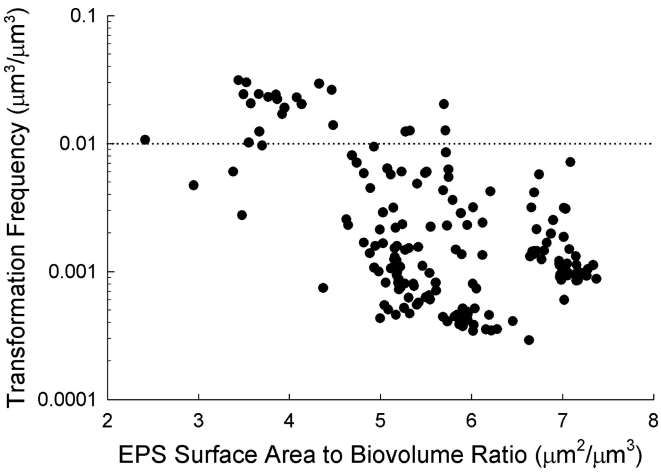

FIG 1 Correlation of transformation frequency and EPS surface area-to-biovolume ratio. The Spearman rank order correlation coefficient, r_s, is −0.42, with a P value of < 0.001. The reference line at 0.01 shows that transformation frequency peaked when the EPS surface area-to-biovolume ratio was greater than 3 $\mu m^2/\mu m^3$ and less than 5 $\mu m^2/\mu m^3$. Each data point represents the result from one scanned location.

TABLE 3 Transformant biovolume Spearman rank order correlation results for significant architectural metrics[a]

Correlation level[b]	Metric(s) with indicated correlation (r_s; P)	
	Positive	Negative
Strong	None	None
Intermediate	EPS biovolume (0.57; <0.001)	EPS porosity (−0.53; <0.001)
Weak	Overall biovolume (0.47; <0.001); EPS surface area (0.44; <0.001); Overall surface area (0.44; <0.001); cellular biovolume (0.43; <0.001); cellular surface area (0.42; <0.001); EPS roughness (0.33; <0.001)	Overall porosity (−0.40; <0.001); cell porosity (−0.36; <0.001); EPS SA:BV (−0.29; <0.001)

[a] Correlations with a P value less than 0.05 were considered to be significant. EPS, extracellular polymeric substances; SA:BV, surface area-to-biovolume ratio.
[b] r_s value were defined to have the following level of correlation: $0.75 \leq r_s < 1$ and $-0.75 \geq r_s > -1$ were strong; $0.50 \leq r_s < 0.75$ and $-0.50 \geq r_s > -0.75$ were intermediate; $0.25 \leq r_s < 0.50$ and $-0.25 \geq r_s > -0.50$ were weak; and $-0.25 < r_s < 0.25$ had no correlation.

DISCUSSION

We investigated whether monoculture *A. baylyi* biofilm architecture—in terms of cellular, EPS and their combined characteristics—influences the efficiency of gene transfer by transformation.

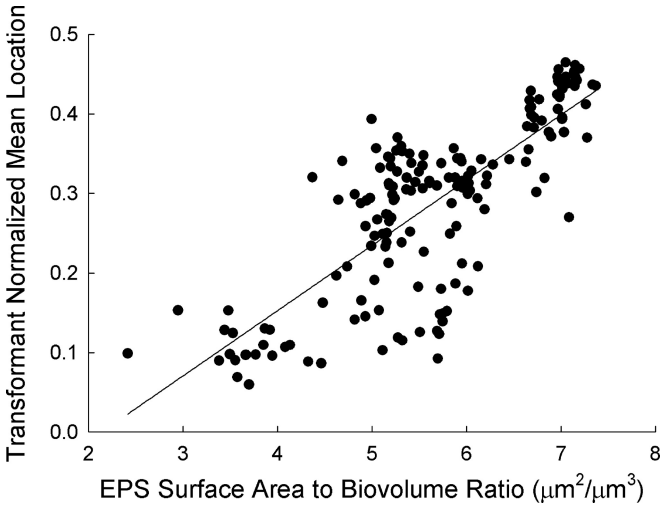

FIG 2 Distribution of transformant normalized mean location as a function of EPS surface area-to-biovolume ratio. The Spearman rank order correlation coefficient, r_s, is 0.75 with a P value of <0.001. Each data point represents the result from one scanned location. The regression line has the equation $y = -0.176 + 0.082x$, with an R^2 value of 0.62. NML values near 0 indicate biomass near the substratum, while values close to 1 indicate biomass close to the bulk medium interface.

TABLE 4 Transformant NML Spearman rank order correlation results for significant architectural metrics[a]

Correlation level[b]	Metric(s) with indicated correlation (r_s; P)	
	Positive	Negative
Strong	EPS SA:BV (0.75; <0.001)	None
Intermediate	EPS porosity (0.63; <0.001); EPS NML (0.55; <0.001); EPS total spreading (0.54; <0.001); EPS vertical spreading (0.50; <0.001)	None
Weak	Overall vertical spreading (0.45; <0.001); maximum thickness (0.45; <0.001); cellular vertical spreading (0.44; <0.001); overall SA:BV (0.43; <0.001); overall NML (0.43; <0.001); cellular mean thickness (0.41; <0.001); cellular NML (0.40; <0.001); EPS horizontal spreading (0.39; <0.001); overall mean thickness (0.38; <0.001); overall porosity (0.38; <0.001); overall total spreading (0.28; <0.001); cellular porosity (0.28; <0.001); EPS mean thickness (0.27; <0.001); cellular total spreading (0.26; <0.001)	EPS biovolume (−0.40; <0.001); 3D coloc cellular EPS (−0.26; <0.001)

[a] Correlations with a P value less than 0.05 were considered to be significant. 3D coloc cellular EPS, three-dimensional colocalization of cellular-and-EPS; EPS, extracellular polymeric substances; NML, normalized mean location; SA:BV, surface area to biovolume ratio.
[b] r_s values were defined to have the following level of correlation: $0.75 \leq r_s < 1$ and $-0.75 \geq r_s > -1$ were strong; $0.50 \leq r_s < 0.75$ and $-0.50 \geq r_s > -0.75$ were intermediate; $0.25 \leq r_s < 0.50$ and $-0.25 \geq r_s > -0.50$ were weak; and $-0.25 < r_s < 0.25$ had no correlation.

Previous studies have implicated the high cell density of biofilms as a major influence on transformation efficiency (21, 28, 29). Li et al. (28) showed that natural genetic transformation was 10 to 600 times more frequent in *Streptococcus mutans* biofilms than in planktonic cultures. Additionally, Hendrickx et al. (21) showed that transformation is detectable in *A. baylyi* biofilms with a concentration as low as 1 fg of plasmid DNA per ml. The present study demonstrates that *A. baylyi* biofilm architecture has a varying degree of influence on transformation frequency, transformant volume, and transformant location.

Because nutrient conditions are known to influence natural com-

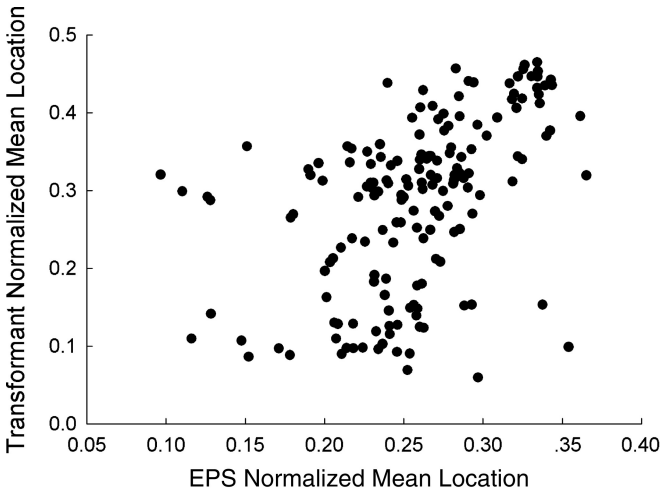

FIG 3 Correlation of transformant normalized mean location and EPS normalized mean location. The Spearman rank order correlation coefficient, r_s, is 0.55, with a P value of < 0.001. Each point represents the result from one scanned location. NML values near 0 indicate biomass near the substratum, while values close to 1 indicate biomass close to the bulk medium interface.

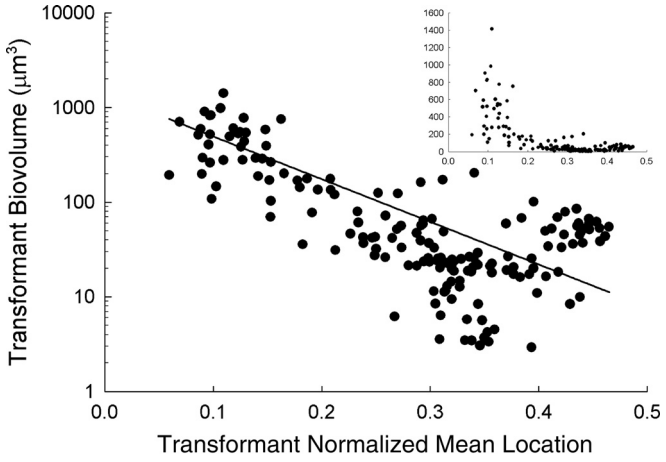

FIG 4 The distribution of transformant biovolume as a function of transformant normalized mean location. Most transformants were found close to the substratum. Each point represents the result from one scanned location. The regression line has the equation $y = 1{,}395.6e^{-10.4}$ with an R^2 value of 0.59. The inset contains the same data but on a linear scale to emphasize the peak in transformant biovolume when the NML was between 0.1 and 0.2. Normalized mean location values near 0 indicate biomass near the substratum, while values close to 1 indicate biomass close to the bulk medium interface.

petence (6, 30–32), biofilms in this study were washed prior to transformation to avoid growth medium-induced competence variability. Perumbakkam et al. (33) and Hendrickx et al. (21) previously showed that transformants were most abundant in areas with high cellular density. Corresponding to results from Hendrickx et al., transformation biovolume in this study peaked near the biofilm substratum (Fig. 4), which typically had high cell densities (Fig. 5). However, transformant biovolume had a greater positive correlation with EPS and overall biovolume than with cellular biovolume (Table 3), suggesting that cell density is not the major factor governing the occurrence of transformation and that transformants may not be randomly distributed in the biofilm. Unlike in planktonic cultures, development of competency will be affected by a cell's location in a biofilm, which may be at a different growth stage than other cells in the biofilm or may be experiencing different substrate concentrations. Notably, EPS architecture was not measured in the investigations performed by Perumbakkam et al. (33) and Hendrickx et al. (21). Specifically, competency may not be uniform throughout the biofilm but may develop in some subpopulations but not others, leading to the phenomenon of bistability (34). This phenomenon may have played a role in the biofilms that did not have significantly different architectures but did have different transformation frequencies.

Of the three biovolume metrics, EPS biovolume had the greatest Spearman rank order correlation with transformant biovolume (Table 3). Although transformant biovolume was not strongly correlated with any architectural metrics, the two metrics with the greatest Spearman rank order correlation were a measure of EPS architecture. The importance of EPS architecture is also apparent in its influence on transformant NML, where the top five correlated metrics were also measures of EPS architecture (Table 4). In particular, EPS surface area-to-biovolume ratio had the greatest Spearman rank order correlation to both transformation frequency (Table 2) and transformation NML (Table 4).

While BD4 has been described as being highly competent (16), to our knowledge the transformation efficiency of BD4 planktonic cultures or biofilms has not previously been quantified. Historically, the miniencapsulated ADP1 has been used for experimentation due to its ease of use in liquid cultures; the copiously capsulated BD4 can be problematic in protocols requiring centrifugation because it does not pellet sufficiently. Although it has been shown that the capsule of BD4 does not prevent transformation (16), we hypothesized that its capsulation would reduce transformation frequency. Kaplan and Rosenberg (35) showed that BD4 produces four times the amount of the primary capsular polysaccharide component, L-rhamnose, that ADP1 does. While these results were obtained using liquid cultures, similar differences in EPS production were also observed in biofilms in this study, where BD4 EPS biovolume was typically twice that of ADP1 biofilms. However, despite increased EPS, a BD4 biofilm had the second greatest average transformation frequency (Table 1).

The major role of EPS may be facilitating the binding and stabilization of plasmid DNA for cellular uptake. Specifically, an optimized ratio of EPS surface area to biovolume was necessary to enhance transformation frequency (Fig. 1). A high ratio value increases interconnecting channels, which can facilitate transport to deeper biofilm regions (10, 11). However, a high surface area also increases the chances of plasmid DNA adhesion close to the bulk medium interface

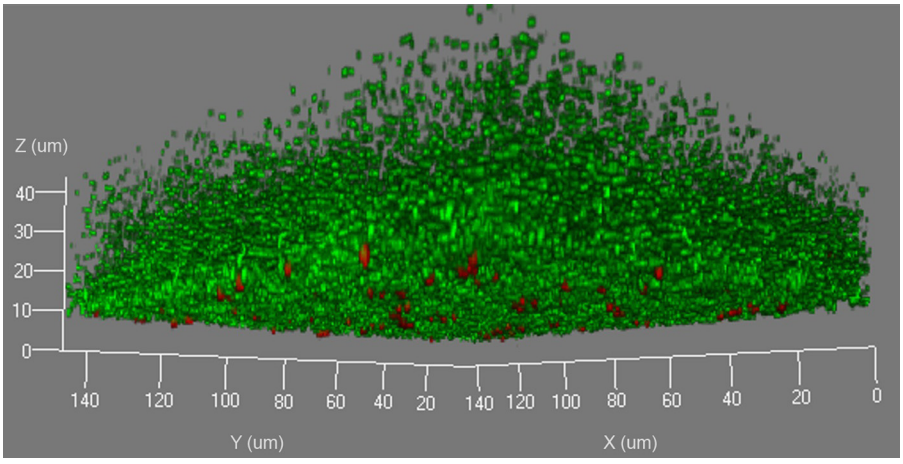

FIG 5 Confocal laser scanning microscope image looking up from below the substratum of an ADP1 biofilm grown in brain heart infusion medium. This image shows that transformants (red) are localized primarily at the substratum of the biofilm. Cellular biomass is shown in green.

before the DNA can penetrate into the biofilm. As a result, when the ratio increases, transformants are found closer to the bulk medium interface (Fig. 2). The lower observed volume of transformants at the biofilm-bulk liquid interface may be a result of cellular erosion (36).

In conclusion, the main effect of EPS on natural transformation in biofilms is due to its architectural characteristics and not the relative amount of EPS present. This effect of EPS architecture on transformation may also be apparent in biofilms of other *A. baylyi* strains, which have been characterized as being highly competent (17). Future research quantifying the amount of retained DNA based on biofilm architecture would further benefit this area of study.

ACKNOWLEDGMENTS

R.T.M. was partially funded by an industry-supported fellowship under the Training Program in Biomolecular Technology at the University of California, Davis, and by the NEAT-IGERT program, sponsored by the National Science Foundation (IGERT grant DGE-9972741).

REFERENCES

1. **Hara T, Ueda S.** 1981. A study on the mechanism of DNA excretion from *P. aeruginosa* KYU-1: effect of mitomycin-C on extracellular DNA production. Agric. Biol. Chem. **45:**2457–2461. http://dx.doi.org/10.1271/bbb1961.45.2457.
2. **Whitchurch CB, Tolker-Nielsen T, Ragas PC, Mattick JS.** 2002. Extracellular DNA required for bacterial biofilm formation. Science **295:**1487–1487. http://dx.doi.org/10.1126/science.295.5559.1487.
3. **Steinberger RE, Holden PA.** 2005. Extracellular DNA in single- and multiple-species unsaturated biofilms. Appl. Environ. Microbiol. **71:**5404–5410. http://dx.doi.org/10.1128/AEM.71.9.5404-5410.2005.
4. **Gerischer U (ed).** 2008. *Acinetobacter*: molecular biology. Caister Academic Press, Norfolk, United Kingdom.
5. **Hendrickx L, Wuertz S.** 2004. Investigating *in situ* natural genetic transformation of *Acinetobacter* sp. BD413 in biofilms with confocal laser scanning microscopy, p 159–173. *In* Setlow JK (ed), Genetic engineering: principles and methods, vol 26. Kluwer Academic/Plenum Publishers, New York, NY. http://dx.doi.org/10.1007/978-0-306-48573-2_9.
6. **Nielsen KM, Bones AM, van Elsas JD.** 1997. Induced natural transformation of *Acinetobacter calcoaceticus* in soil microcosms. Appl. Environ. Microbiol. **63:**3972–3977.
7. **Palmen R, Buijsman P, Hellingwerf KJ.** 1994. Physiological regulation of competence induction for natural transformation in *Acinetobacter calcoaceticus*. Arch. Microbiol. **162:**344–351. http://dx.doi.org/10.1007/BF00263782.
8. **Lewandowski Z, Beyenal H.** 2003. Mass transport in heterogeneous biofilms, p 147–175. *In* Wuertz S, Bishop PL, Wilderer PA (ed), Biofilms in wastewater treatment. IWA Publishing, London, United Kingdom.
9. **Picioreanu C, van Loosdrecht MCM, Heijnen JJ.** 2000. A theoretical study on the effect of surface roughness on mass transport and transformation in biofilms. Biotechnol. Bioeng. **68:**355–369. http://dx.doi.org/10.1002/(SICI)1097-0290(20000520)68:4<355::AID-BIT1>3.0.CO;2-A.
10. **Massol-Deya AA, Whallon J, Hickey RF, Tiedje JM.** 1995. Channel structures in aerobic biofilms of fixed-film reactors treating contaminated groundwater. Appl. Environ. Microbiol. **61:**769–777.
11. **Okabe S, Kuroda H, Watanabe Y.** 1998. Significance of biofilm structure on transport of inert particulates into biofilms. Water Sci. Technol. **38:**163–170. http://dx.doi.org/10.1016/S0273-1223(98)00690-8.
12. **Bishop PL, Kinner NE.** 1986. Aerobic fixed-film processes, p 113–176. *In* Schoenborn W (ed), Biotechnology: a comprehensive treatise, vol 8. VCH Publishers, New York, NY.
13. **Stoodley P, Sauer K, Davies DG, Costerton JW.** 2002. Biofilms as complex differentiated communities. Annu. Rev. Microbiol. **56:**187–209. http://dx.doi.org/10.1146/annurev.micro.56.012302.160705.
14. **Czaczyk K, Myszka K.** 2007. Biosynthesis of extracellular polymeric substances (EPS) and its role in microbial biofilm formation. Pol. J. Environ. Stud. **16:**799–806. http://www.pjoes.com/pdf/16.6/799-806.pdf.
15. **Flemming HC, Wingender J.** 2003. The crucial role of extracellular polymeric substances in biofilms, p 178–210. *In* Wuertz S, Bishop PL, Wilderer PA (ed), Biofilms in wastewater treatment. IWA Publishing, London, United Kingdom.
16. **Juni E, Janik A.** 1969. Transformation of *Acinetobacter calco-aceticus* (*Bacterium anitratum*). J. Bacteriol. **98:**281–288.
17. **Vaneechoutte M, Young DM, Ornston LN, De Baere T, Nemec A, Van Der Reijden T, Carr E, Tjernberg I, Dijkshoorn L.** 2006. Naturally transformable *Acinetobacter* sp strain ADP1 belongs to the newly described species *Acinetobacter baylyi*. Appl. Environ. Microbiol. **72:**932–936. http://dx.doi.org/10.1128/AEM.72.1.932-936.2006.
18. **Labes M, Puhler A, Simon R.** 1990. A new family of RSF1010-derived expression and *lac*-fusion broad-host-range vectors for gram-negative bacteria. Gene **89:**37–46. http://dx.doi.org/10.1016/0378-1119(90)90203-4.
19. **Hendrickx L.** 2002. Natural genetic transformation in *Acinetobacter* sp. BD413 biofilms: introducing natural genetic transformation as a tool for bioenhancements of biofilm reactors. Thesis. Technical University of Munich, Munich, Germany.
20. **Sambrook J, Fritsch EF, Maniatis T.** 1989. Molecular cloning: a laboratory manual, 2nd ed. Cold Spring Harbor Laboratory, Cold Spring Harbor, NY.
21. **Hendrickx L, Hausner M, Wuertz S.** 2003. Natural genetic transformation in monoculture *Acinetobacter* sp. strain BD413 biofilms. Appl. Environ. Microbiol. **69:**1721–1727. http://dx.doi.org/10.1128/AEM.69.3.1721-1727.2003.
22. **GrayMerod R, Hendrickx L, Mueller LN, Xavier JB, Wuertz S.** 2005. Effect of nucleic acid stain Syto9 on nascent biofilm architecture of *Acinetobacter* sp. BD413. Water Sci. Technol. **52:**195–202.
23. **Hoch HC, Galvani CD, Szarowski DH, Turner JN.** 2005. Two new fluorescent dyes applicable for visualization of fungal cell walls. Mycologia **97:**580–588. http://dx.doi.org/10.3852/mycologia.97.3.580.
24. **Korber DR, Lawrence JR, Hendry MJ, Caldwell DE.** 1992. Programs for determining statistically representative areas of microbial biofilms. Binary Comput. Microbiol. **4:**204–210.
25. **Sekar R, Griebe T, Flemming HC.** 2002. Influence of image acquisition parameters on quantitative measurements of biofilms using confocal laser scanning microscopy. Biofouling **18:**47–56. http://dx.doi.org/10.1080/08927010290017725.
26. **Merod RT, Warren JE, McCaslin H, Wuertz S.** 2007. Toward automated analysis of biofilm architecture: bias caused by extraneous confocal laser scanning microscopy images. Appl. Environ. Microbiol. **73:**4922–4930. http://dx.doi.org/10.1128/AEM.00023-07.
27. **Mueller LN, de Brouwer JF, Almeida JS, Stal LJ, Xavier JB.** 2006. Analysis of a marine phototrophic biofilm by confocal laser scanning microscopy using the new image quantification software PHLIP. BMC Ecol. **6:**1. http://dx.doi.org/10.1186/1472-6785-6-1.
28. **Li YH, Lau PCY, Lee JH, Ellen RP, Cvitkovitch DG.** 2001. Natural genetic transformation of *Streptococcus mutans* growing in biofilms. J. Bacteriol. **183:**897–908. http://dx.doi.org/10.1128/JB.183.3.897-908.2001.
29. **Molin S, Tolker-Nielsen T.** 2003. Gene transfer occurs with enhanced efficiency in biofilms and induces enhanced stabilisation of the biofilm structure. Curr. Opin. Biotechnol. **14:**255–261. http://dx.doi.org/10.1016/S0958-1669(03)00036-3.
30. **Nielsen KM, van Weerelt MDM, Berg TN, Bones AM, Hagler AN, van Elsas JD.** 1997. Natural transformation and availability of transforming DNA to *Acinetobacter calcoaceticus* in soil microcosms. Appl. Environ. Microbiol. **63:**1945–1952.
31. **Palmen R, Vosman B, Buijsman P, Breek CKD, Hellingwerf KJ.** 1993. Physiological characterization of natural transformation in *Acinetobacter calcoaceticus*. J. Gen. Microbiol. **139:**295–305. http://dx.doi.org/10.1099/00221287-139-2-295.
32. **Paul JH, Frischer ME, Thurmond JM.** 1991. Gene-transfer in marine water column and sediment microcosms by natural plasmid transformation. Appl. Environ. Microbiol. **57:**1509–1515.
33. **Perumbakkam S, Hess TF, Crawford RL.** 2006. A bioremediation approach using natural transformation in pure-culture and mixed-population biofilms. Biodegradation **17:**545–557. http://dx.doi.org/10.1007/s10532-005-9025-7.
34. **Dubnau D, Losick R.** 2006. Bistability in bacteria. Mol. Microbiol. **61:**564–572. http://dx.doi.org/10.1111/j.1365-2958.2006.05249.x.
35. **Kaplan N, Rosenberg E.** 1982. Exopolysaccharide distribution of and bioemulsifier production by *Acinetobacter calcoaceticus* BD4 and BD413. Appl. Environ. Microbiol. **44:**1335–1341.
36. **Morgenroth E.** 2003. Detachment: an often-overlooked phenomenon in biofilm research and modeling, p 264–290. *In* Wuertz S, Bishop PL, Wilderer PA (ed), Biofilms in wastewater treatment. IWA Publishing, London, United Kingdom.